01 Jan 2023

Residual Stress Distribution, Distortion, And Crack Initiation In Conventional And Intensive Quench Practices

Kingsley Tochukwu Amatanweze

Mario F. Buchely
Missouri University of Science and Technology, buchelym@mst.edu

Viraj Ashok Athavale

Laura Bartlett
Missouri University of Science and Technology, lnmkvf@mst.edu

et. al. For a complete list of authors, see https://scholarsmine.mst.edu/matsci_eng_facwork/3279

Recommended Citation

K. T. Amatanweze et al., "Residual Stress Distribution, Distortion, And Crack Initiation In Conventional And Intensive Quench Practices," *Journal of Materials Engineering and Performance*, Springer; ASM International, Jan 2023.
The definitive version is available at https://doi.org/10.1007/s11665-023-08985-0

JMEPEG
https://doi.org/10.1007/s11665-023-08985-0

1059-9495/$19.00

ORIGINAL RESEARCH ARTICLE

Residual Stress Distribution, Distortion, and Crack Initiation in Conventional and Intensive Quench Practices

Kingsley Tochukwu Amatanweze, Mario F. Buchely, Viraj Ashok Athavale, Laura N. Bartlett, Ronald J. O'Malley, and Toshi Suzuki

Submitted: 11 June 2023 / Revised: 20 September 2023 / Accepted: 23 October 2023

This study evaluates the effect of two different quench practices on distortion, sensitivity to quench cracking, development and distribution of residual stress, microstructural uniformity, and hardenability of standardized test castings. Navy C-rings made of AISI 4340 were quenched in this experiment. Some rings were quenched in a conventional draft tube immersion quench bath, and others were quenched in an intensive quench spray system to compare with the results from the conventional immersion quench bath. The rings were measured with a coordinate measuring machine, for distortion and flatness, before and after quenching. Hardness profiles of the quenched rings showed through hardness of 57.0-59.0 HRC, and the microstructures were largely martensitic. DANTE modeling software was used to predict the quenched properties of the rings, simulating microstructural transformation and residual stresses for each quench practice. XRD was used to measure surface residual stress distribution of the quenched rings, and results were compared to the predicted values by the modeling software. The surface residual stress was tensile for the conventional immersion quench and compressive for the intensive spray quench. Crack initiation correlated to areas of large tensile stress concentration and microstructural heterogeneity.

Keywords cos α XRD technique, finite element method, heat transfer coefficient, intensive quenching, quench distortion, surface residual stress

1. Introduction

Quenching is a heat treatment procedure commonly used to achieve hardness in steels. It involves heating the metal to a high temperature known as the austenitization temperature and holding it at that temperature for a duration of time before rapidly cooling it in a quenching medium. The steel is held at the austenitization temperature for a time long enough to form a homogenous single-phase solid solution, before quenching rapidly enough to avoid transformation of the austenite to a stable phase. Metastable martensite is formed instead, which is relatively hard and brittle (Ref 1-3). This transformation of austenite to martensite is diffusionless and lattice-displacive. Quenching processes include immersion, film, gas, and spray quenching. Quenching, which involves the transfer of heat from the hot work piece to the quenching medium, propels microstructural transformation, and stress and strain development in the material. A thermal gradient is created on the surface of the quenched material during quenching because of the variance in heat transfer at different locations on the surface and within. The difference in thermal expansion causes unequal shrinkage on the material and results in thermal stress, while volume expansion from phase transformation leads to transformation stress. The sum of all the stress in the material is referred to as the residual stress (Ref 2, 4). The quenched material deforms or cracks when the effective stress exceeds its strength (Ref 1, 2). Hence, quench distortion and cracking are the two main defects of quenching, causing serious concern in heat treatment industries. Tensile residual stress in a material would result in dimensional instability and a reduction in service life. High residual compressive stress on the other hand improves component's life span by enhancing wear resistance, corrosion resistance, and fatigue life (Ref 2, 4, 5). This highlights the importance of evaluating the residual stress distribution in a material during and after quenching.

Additionally, there has been a sustained interest in the simulation of heat treatment in industries, especially quench residual stress and distortion. Modeling techniques have become more robust, improving from two-dimensional to three-dimensional finite element analysis, and utilizing the interaction of multiple physical phenomena (Ref 6-8). Many of the simulation results from the literature agree with experimental results especially on phase transformation, hardness, and residual stress distribution. Simulations on distortion also showed agreement, though qualitatively (Ref 7, 8).

The spray quench bath used in this study employs the intensive quench technique. The pump pressure of the spray nozzles was 170-180 psi (1.17-1.24 Mpa), high enough to produce a cooling rate greater than the critical cooling rate of the material above which the cracking tendency decreases.

This invited article is part of a special topical issue of the *Journal of Materials Engineering and Performance* on Residual Stress Analysis: Measurement, Effects, and Control. The issue was organized by Rajan Bhambroo, Tenneco, Inc.; Lesley Frame, University of Connecticut; Andrew Payzant, Oak Ridge National Laboratory; and James Pineault, Proto Manufacturing on behalf of the ASM Residual Stress Technical Committee.

Kingsley Tochukwu Amatanweze, Mario F. Buchely, Viraj Ashok Athavale, Laura N. Bartlett, and **Ronald J. O'Malley**, Missouri University of Science and Technology, Rolla, MO; and **Toshi Suzuki**, Pulstec USA, Inc., Novi, MI. Contact e-mail: ktanbz@mst.edu.

Published online: 28 November 2023

Even though the probability of part cracking increases with an increasing cooling rate, Kobasko reported that cooling rate above 470 °C/s decreases quench cracking tendency in the quenched sample and this is referred as intensive quenching (Ref 1, 5, 9-12). Hence, part cracking would be prevented if quenching is done properly with high cooling rate within martensite range (Ref 11, 12). The intensive quenching technique has Grossmann quench severity number greater than 6 (Ref 2, 13) and a 20,000-50,000 W/m2K heat transfer coefficient (Ref 2). The technique suppresses film boiling and nucleate boiling and cools samples uniformly with a very high cooling rate, hence, instantaneously simultaneous transforming of the austenite to martensite across the entire surface and producing a high surface compressive stress (Ref 2, 3, 5, 9-12, 14). This hard martensite shell at the surface is put in compression by the thermal shrinkage of austenite at the core of the sample. Surface compressive stress results in minimum distortion, lower probability of cracking, enhanced mechanical properties, and improved fatigue/service life (Ref 2, 4, 5, 9, 11-13, 15). Complex castings that have thick and thin sections are notoriously difficult to quench without distortion and cracking. This problem is exacerbated in the case of medium carbon alloy steels. During intensive quenching, complex castings with varying section thickness undergo immediate and uniform martensite transformation over the entire part surface, minimizing tensile stress due to nonuniform transformation and cooling (Ref 10, 11). The Navy C-ring is a standard part design that has thick and thin sections and is used to measure distortion and cracking potential during heat treatment (Ref 16-21). Yu et al. in their distortion study using AISI 4140 steel reported that the opening of the C-ring gap during quenching was because of the higher volume fraction of martensite formed at the thinner section which is less dense than the mix of martensite and lower bainite also formed at the thick section of the ring (Ref 20).

This present work evaluates the effect of two different quench practices on distortion, sensitivity to quench cracking, development and distribution of residual stress, and microstructural uniformity of a complex standardized part. These quench properties were studied on AISI 4340 steel Navy C-rings quenched in both draft tube immersion bath and in an intensive quench spray tank designed and custom built at Missouri S&T. The quenching processes were also modeled on DANTE, a commercially available heat treatment simulation software based on finite element modeling. The experimental results were compared with DANTE modeling predictions.

2. Materials and Method

Navy C-rings of thickness of 25.4 mm (1.0 inch) and external diameter of 127 mm (5.0 inches) (Fig. 1a) were machined from a 177.8 mm (7.0in) × 177.8 mm(7.0in) × 553.7 (21.5in) AISI 4340 billet (Fig. 2a). The billet was cast, and C-rings were sectioned from the same location to ensure consistent material properties in all the sectioned rings (Fig. 2b). The machined 4340 steel C-ring parts were each stamped with a specimen ID number and measured before and after heat treatment using a coordinate measuring system (CMM) and using 3D scanning to precisely determine dimensions. CMM was utilized to determine distortion in the Navy C-ring castings and was measured as the change in the fork gap opening along five different points of each side of the fork side plane. These points were utilized to determine the change in distance between the fork gap as shown in Fig. 3(a), (b) and (c) and the method was similar to the one reported in (Ref 22). 15.0 mm (0.59inches) diameter and 165.1 mm (6.5 inches) length bars were welded on the rings for positioning on the support fixtures in the quench baths. Figure 1(b) shows the sectioning location for metallography and hardness measurements of the thick and thin sections of the C-ring. Microstructural analysis and hardness measurements were performed across the thickness of the C-rings and not on their faces.

The carbon and sulfur contents of the AISI 4340 billet were determined using combustion and inert gas fusion analysis on Laboratory Equipment Corporation's LECO TC500 analyzer following ASTM E1019 standards, while the rest of the alloys chemistries was determined using optical emission arc spectroscopy (OES) on an Oxford Instrument. A comprehensive chemistry of the AISI 4340 billet is shown in Table 1.

2.1 Determination of Heat Transfer Coefficient (HTC) Using Temperature Probe

The rings were quenched in two quench systems, (a) a forced convection immersion quench in a draft tube and (b) an intensive quenching in a spray quench tank. The HTC of the two quench systems was determined utilizing a temperature probe made of 304 stainless-steel material. A thermocouple tip was brazed to the center of the probe with a Ni-Ag brazing rod at 950 °C. Using the temperature probe and inverse algorithm, HTC was calculated.

2.2 Heat Treatment Process

C-rings were double wrapped in stainless-steel bags during heating to protect the ring from furnace atmosphere and prevent resultant decarburization. The wrapped rings were austenitized at 920 °C for 1 hour. The stainless-steel bags were removed, and the ring was heated again in the furnace for 10 minutes to regain lost temperature before quenching them in water to room temperature in 2.5 minutes. The quench bath temperature ranged between 20 and 24 °C. The transfer time ranged between 10 to 15 sec. Water flow rate in the draft was $>$ 6ft/s, while the pump pressure of the IQ spray system was 170-180 psi (1.17-1.24Mpa). Figure 4(a) shows the concept drawing of the Missouri S&T IQ facility with the spray manifold system located in the middle of the tank. The cylindrical manifold is hollow on the inside and serves as an accumulator to distribute equal pressure through a series of spray header posts. There are many threaded openings in the manifold that allow for different placement of nozzles depending on the part geometry. And these openings can be blocked off when not in use. Figure 4(b) and (c) shows quenching of the C-ring casting utilizing an array of four nozzles placed orthogonal to one another. This configuration allows for the removal of heat on all sides and edges of the C-ring. The water droplets from the spray nozzles are uniform in size and distributed equally throughout the spray pattern. For the forced convention immersion quench procedure, the draft tube tank was filled with water and was agitated by the help of a propeller positioned inside the tube. In the draft tube system (Fig. 4d), rings were suspended vertically in a clamp, with the thin section just at the mouth of the draft tube. In the spray quench system, rings were fixed vertically in the center of four nozzle stands, each having three spray nozzles.

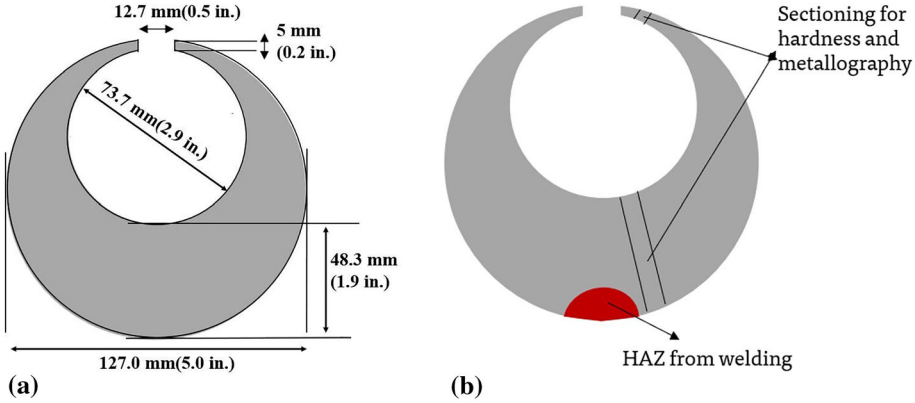

Fig. 1 A sketch of the Navy C-ring used in this study, the (a) dimensions and (b) sectioning for hardness and metallography from the thin section and from the thick section away from the welding heat affected zone (HAZ)

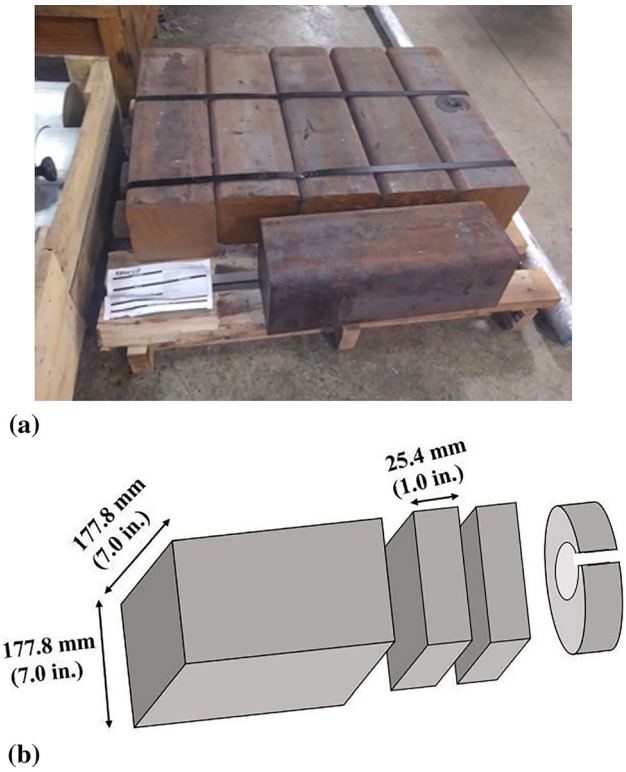

Fig. 2 To reduce variability in chemistry and cooling rates, Navy C-ring castings for the study of intensive quenching in contrast to immersion quenching procedures were sectioned from AISI 4340 billet material produced from the same heat. (a)AISI 4340 billet, (b) schematics of the sectioning of the C-rings from the billet

Rings orientation was maintained at 45° from each spray nozzle (Fig. 4b and c).

2.3 Microstructural Analysis and Hardness Test

Samples from the quenched rings were polished using appropriate metallographic procedure and etched with Nital 2%. The microstructure of the etched samples was studied under an optical microscope. The hardness profile in HRC of the samples was also determined using Wilson hardness testing equipment.

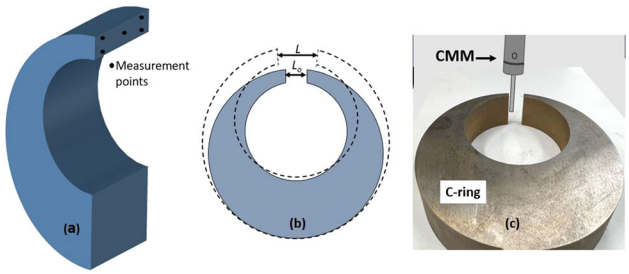

Fig. 3 A common indicator of navy C-ring distortion is a variation in the fork gap opening before and after quenching. A CMM equipment was used to measure five distinct points on the pieces along the inner plane of each fork gap. Shown in the figures are (a) a section of the ring with five distinct measurement points, (b) gap openings of the ring before (L_o) and after (L) quenching, and (c) CMM measurement set up

2.4 Residual Stress Characterization

X-ray Diffraction was used to study experimentally the stress profile in the high stress distribution areas predicted by the modeling software. This was done using Cosα technique (Fig. 5), equally known as single exposure technique, on Pulstec μ-X360 XRD Residual Stress Measurement Equipment. Stress measurements were taken in {211} plane in x-direction, and a tilt angle of 35°. Depth of penetration of the x-ray is 10-15 μm, and the diameter of the beam was 2 mm. x-ray stress measurements were taken on as-quenched surfaces of the rings (there was no significant decarburization on the quenched rings' surfaces). This method, like the $Sin^2\psi$ method, equally obeys the Bragg's diffraction law. The stress was calculated using Young's modulus, *E*, and Poisson's ratio, *V*, of 210.0Gpa and 0.280, respectively.

Tanaka and coworkers developed the Cosα technique (Ref 23). In this technique, the perfectly circular Debye ring from the unstressed specimen is compared with the Debye ring formed by the diffracted beam from the stressed specimen on a two-dimension detector in form of an image plate. The Debye ring loses its circular shape as the specimen undergoes stress. From the variation in diffraction angle caused by the Debye ring's radius, it is possible to calculate the strain. Strain can be calculated here using the following expression (Ref 23-25):

Table 1 Chemical composition of the AISI 4340 billet

Alloy	C	S	Mn	P	Si	Cr	Mo	Ni	Al	Cu	Ti	V
%wt.	0.408	0.0074	0.859	0.055	0.163	1.056	0.297	1.687	0.036	0.214	0.015	0.029

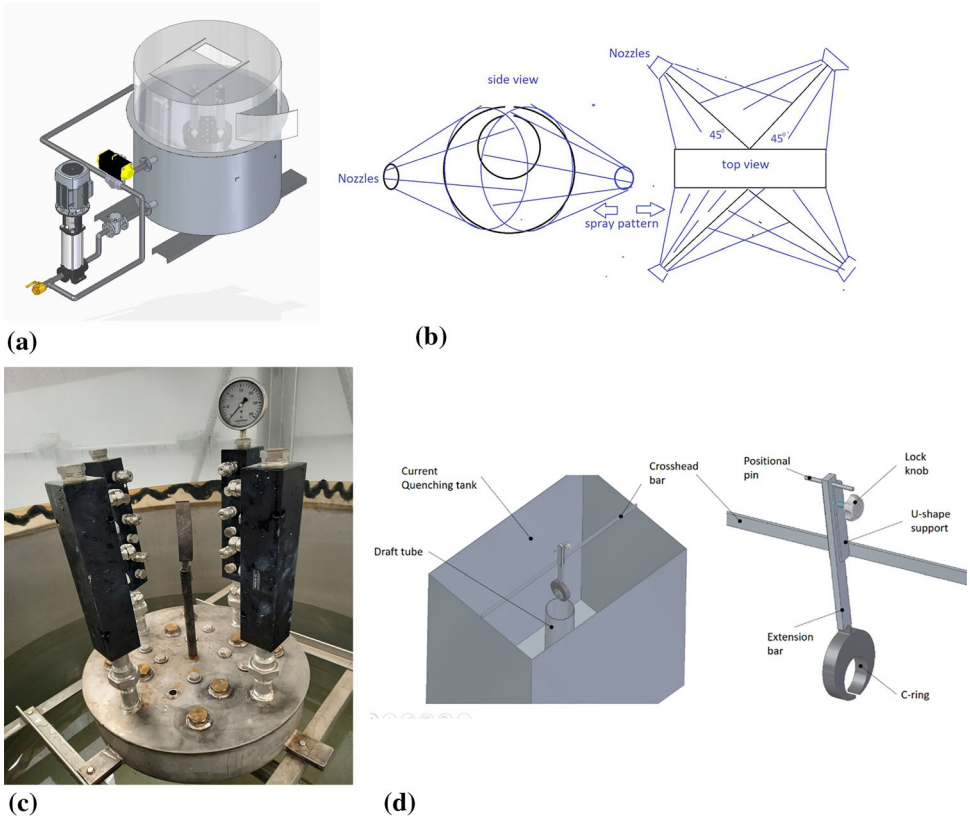

Fig. 4 (a) Final drawing of the Missouri S&T IQ system and the actual finished system located at Missouri S&T. (b) Orientation of the C-ring 45 °C from the spray nozzles, side, and top views of the spray pattern of the nozzles (c) Side view of the C-Ring mounted at the center of the spray nozzles. (d) A schematic diagram of the draft tube system and a C-ring fixture for immersion quenching

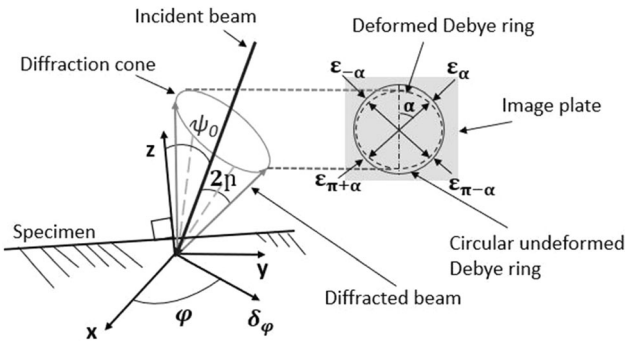

Fig. 5 Illustration of the Cosα stress measurement technique showing the specimen, incident beam, diffracted beam, diffraction cone, Debye rings, image plate, measurement δφ direction, and the d-spacing

$$\bar{\varepsilon}_\alpha = \frac{1}{2}\left[(\varepsilon_\alpha - \varepsilon_{\pi+\alpha}) + (\varepsilon_{-\alpha} - \varepsilon_{\pi-\alpha})\right] \quad \text{(Eq 1)}$$

where the following terms: ε_α, $\varepsilon_{\pi+\alpha}$, $\varepsilon_{-\alpha}$ and $\varepsilon_{\pi-\alpha}$ are strain in four directions calculated from four point located at 90 degree each on the Debye ring. Angle α was varied from 0 to 90° to cover the whole ring. The calculated stress is a linear relationship between stress ($\bar{\varepsilon}_\alpha$) and cos α. Hence, for cos α method, stress is calculated using this equation:

$$\delta_x = -\frac{E}{1+V}\frac{1}{\mathrm{Sin}2\eta \sin 2\psi_0}\frac{\partial \bar{\varepsilon}_\alpha}{\partial \cos\alpha} \quad \text{(Eq 2)}$$

Where E and V are the diffraction's Young's modulus and Poisson's ratio respectively, 2η is the Debye ring semi-angle and is equal to 90-θ_0, while ψ_0 is the angle between incident x-ray and the surface normal. However, to determine the uniaxial

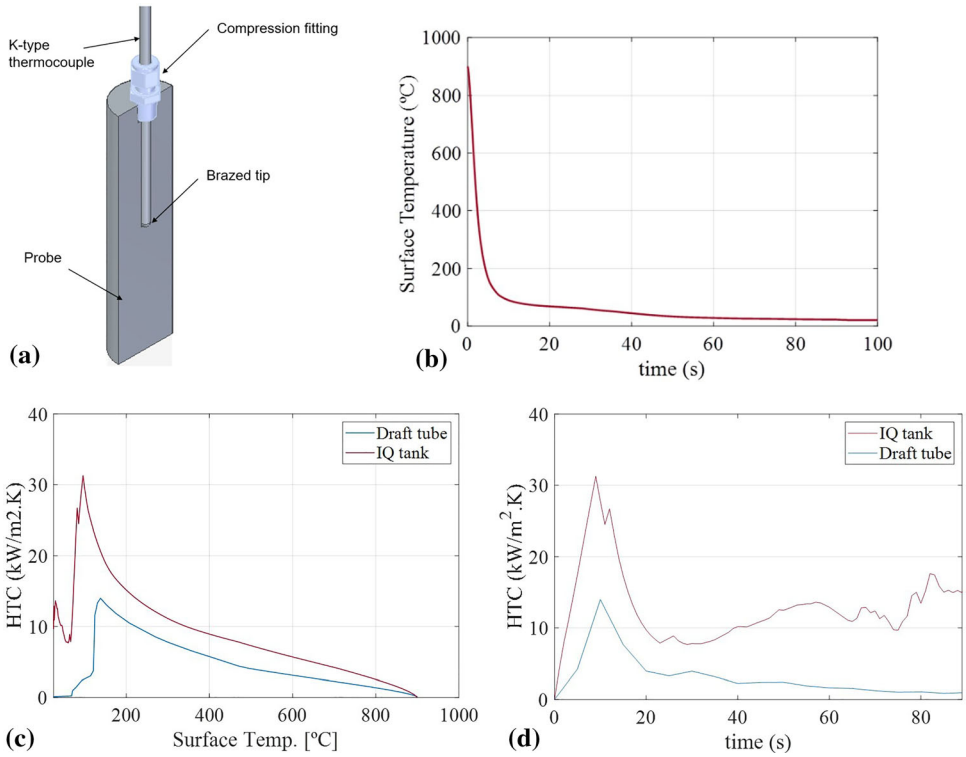

Fig. 6 (a) Schematic of temperature probe in sectional view. The results of the temperature probe experiments from the intensive quench (IQ quench) and draft tube are as shown in the (b) surface temperature against time plot, (c) HTC against surface temperature plot and (d) HTC against cooling time plot. Heat transfer coefficient (HTC) calculated using the temperature probe and the inverse algorithm

stress, the measurements would be taken at angle φ equals to zero (Ref 23-25).

3. Results and Discussion

3.1 Finite Element Modeling

The quench process was modeled by DANTE simulation software, utilizing the quench conditions in the experimental quench. The actual geometry of the C-ring and the chemistry and thermophysical properties of the AISI 4340 steel grade available in the database of the software were used for the simulation. The finite element model was built in Abaqus software. A CAD model of the C-ring was imported from a design software to Abaqus. The part was then meshed utilizing Abaqus meshing tools and using a structured mesh with 8-noded linear hexahedron elements (type C3D8R in Abaqus). A total of 82110 elements were used for a quarter of the C-ring that was modeled and simulated. The computational cooling model was run using the DANTE data embedded in Abaqus. Thermophysical properties of steel are temperature dependent utilizing quadrating interpolation functions. The DANTE database includes experimental TTT curves obtained by dilatometric test. Different phase predictions from the TTT curves are digitalized using Avrami equation (Ref 26, 27):

$$y = 1 - \exp(-\mathrm{kt}^n) \quad \text{(Eq 3)}$$

Where y is the volume fraction of transformed phase, and t is time. n, also known as the Avrami exponent, is a constant related to nucleation and growth, while k is a reaction rate constant. The parameters k and n are temperature dependent constants, and they are adjusted at the 3rd degree polynomial equation to iterate during a time step. Rule of additivity is utilized to transform the TTT curve to a cooling transformation curve for every time step during the simulation process. For martensite formation, a Koistinen–Marburger's relation is utilized (Ref 26, 27):

$$y = 1 - \exp(-\alpha(M_s - T)) \quad \text{(Eq 4)}$$

where M_s is the martensite start temperature, T is the temperature and α is a material constant for the steel. The M_s was calculated according to empirical equation, based on the composition of the steel and its prior austenitic grain size. Volume changes are considered in the simulation and included for the structural calculation of the stresses. The values of volume changes are based on the experimental dilatometric data available in the DANTE database, and corrected for the simulation, based on phase transformation.

The main variable in the simulation for the two quench practices was their rates of heat transfer. The temperature probe experiment showed that the HTC produced in the intensive (spray) quench tank and the draft tube quench bath reached a maximum of about 30,000 and 14,000 W/m^{2}K, respectively (Fig. 6a and b). HTC increases as the wetting front velocity increases. The more vigorously the cooling, the more the magnitude of HTC (Ref 2). Figure 6(b) shows that surface temperature decreases with time. The sectional view of the temperature probe is shown in Fig. 6(a).

DANTE database includes experimental data of dilatometer and Jominy quenching testing for the steel selected. Using the dilatometric expansion during transformation, volumetric

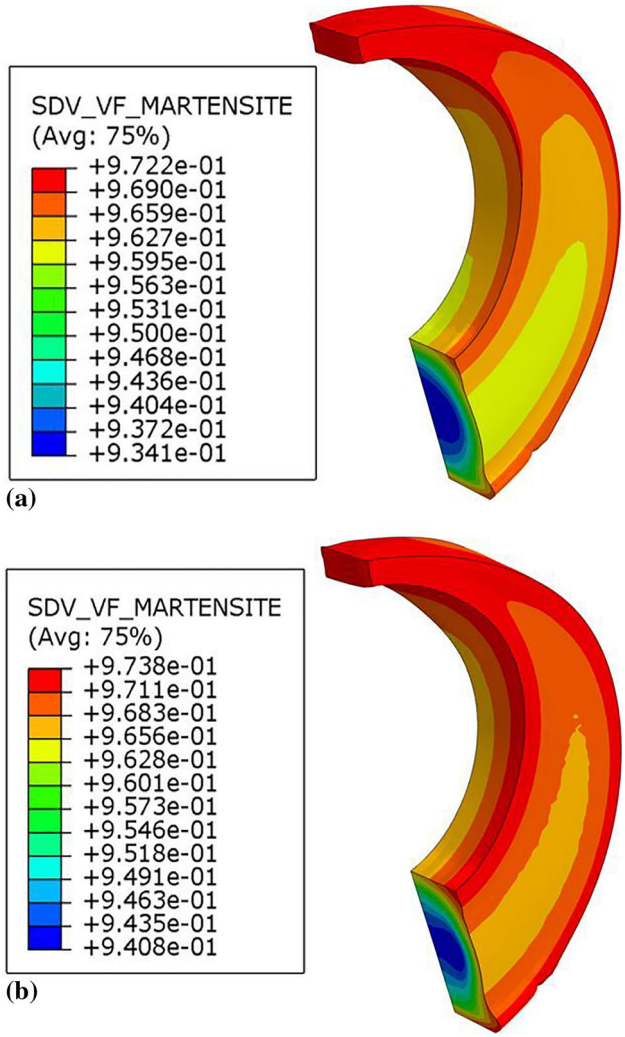

Fig. 7 Volume fraction of martensite transformation prediction from DANTE modeling for (a) draft tube immersion quench and (b) intensive quench conditions.

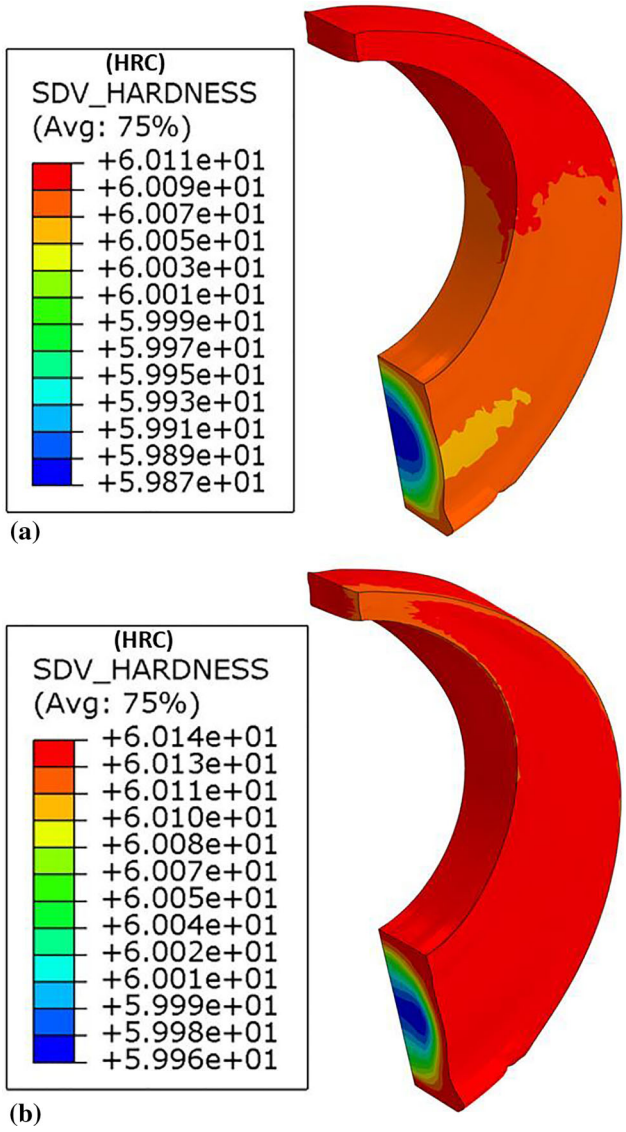

Fig. 8 Hardness (HRC) of the two quench conditions profile as predicted in DANTE modeling shows a very narrow range of hardness between the surface and the core, indicating through hardening of the C-rings for (a) draft tube immersion quench and (b) intensive quench conditions

changes can be calculated, using the theoretical martensite lattice parameters. For the hardness calculation, the Jominy data are calibrated for different cooling rates and impact severities according to the ASTM A255-20 standard. Hardness data are then interpolated for different temperatures and corrected according to the phase fraction of each phase, that is also calculated in the DANTE model, as explained before. DANTE modeling predicted about 97 and 94% martensite on the surface and core of rings in both intensive quench and draft tube quench conditions, respectively (Fig. 7). The intensive quench condition showed a rather insignificant more volume fraction of martensite compared to the draft tube condition. The model also predicted a through hardness of approximately 60 HRC with difference in surface and core hardness around 0.2 HRC for both intensive quench and conventional immersion quench conditions (Fig. 8).

Figure 9(a) and (b) shows the residual stress distribution modeling result of the rings when quenched using conventional immersion quench and intensive quench conditions, respectively. The modeling software predicted an area of high tensile residual stress distribution along the bends flanking the inner circle of the ring (Fig. 9). This could be because of increased bending moments along the curves. These areas of high tensile residual stress profile on the surface of the ring correlated with the areas of crack initiation in some quenched rings. The core of the two conditions was generally under compression. High tensile residual stress was predicted for the surface of the draft tube condition (Fig. 9a), compared to the intensive quench condition which had the ring surface mainly covered by compressive residual stress (Fig. 9b).

The simulation also showed a distortion in shape in the two conditions. While the C-ring gap contracted more along the x-direction in the draft tube modeling, it was observed to have expanded more along the z-direction in the intensive quench modeling (Fig. 10). Displacement in x and z-directions was 0.22 and 0.16 mm in the draft tube and 0.11 and 0.25 mm in the intensive quench modeling, respectively. The draft tube modeling showed more average distortion, 1.7% (%change in

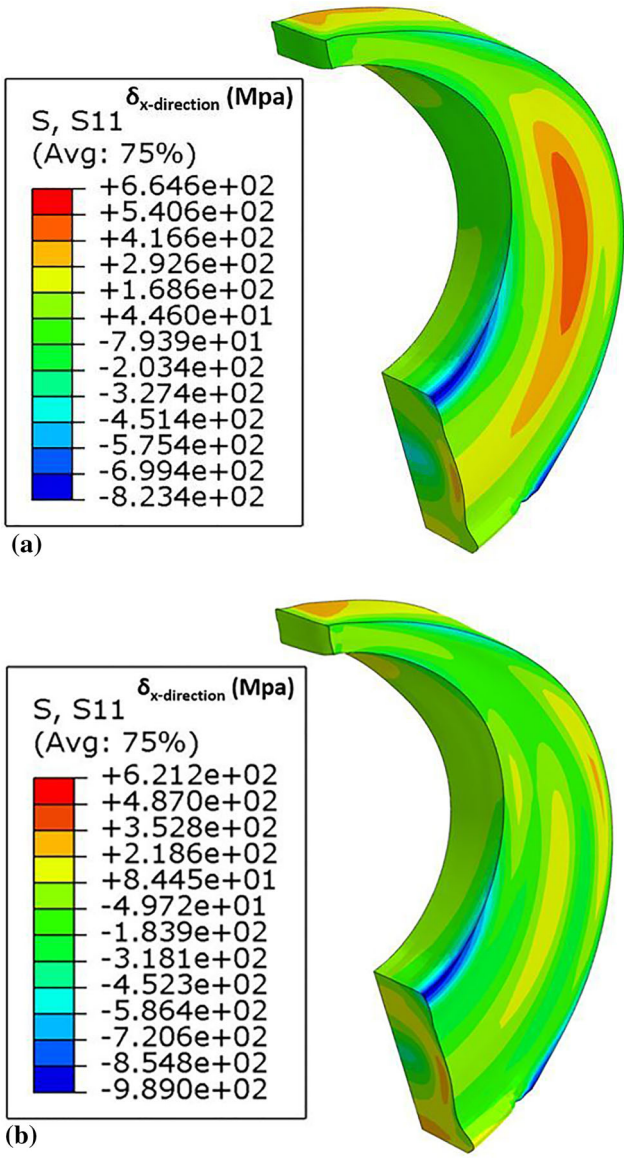

Fig. 9 Residual Stress (Mpa) distribution in the x-direction predicted in DANTE modeling for the (a) draft tube immersion quench and (b) intensive quench conditions

the fork gap opening) in the x-direction, compared to the spray quench modeling result, 0.9%.

3.2 Experimental Results

The microstructure of the samples viewed under an optical microscope showed a martensite structure for the two conditions (Fig. 11), agreeing with the results from the DANTE simulation. The average hardness of the rings was 56.9 ± 1.13 HRC and 58.4 ± 0.52 HRC for the draft tube and intensive quench samples, respectively. The experimental result agreed with the modeling result, with a more consistent hardness profile across the bottom thickness of the ring in the intensive quench sample (Fig. 12).

3.3 X-ray Diffraction

The cos α XRD technique was used to measure surface residual stress distribution in two quench trials (T1 and T2)

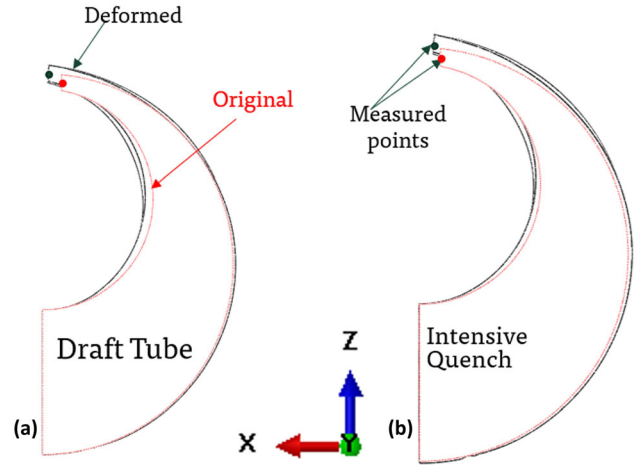

Fig. 10 DANTE prediction for shape distortion in the (a) draft tube immersion quench and (b)intensive quench conditions

conducted with similar quench conditions, and it was determined that a samples stress relieved at 600 °C for 1 hour and cooled in the furnace, showed a mix of low surface tensile and compressive residual stresses ranged from − 21 to 77Mpa, while the spray quenched samples showed consistent high surface compressive residual stress distribution across the tested positions (Fig. 13a), ranging from − 1 to − 322Mpa. However, slightly higher all surface tensile residual stress distribution were observed in the draft tube quenched samples, ranged from 10Mpa to 181Mpa. The experimental residual stress results obtained using Pulstec cos α XRD technique measuring equipment (Fig. 13b) is shown in Fig. 13(c). C-rings measured had no quench cracks.

The residual stress results from XRD agreed with the DANTE modeling predictions, though qualitatively. The model predicted predominance of surface tensile and compressive residual stress in the draft tube immersion quench and intensive quench, respectively, and this agreed with the experimental results. However, the measured tensile stress values were much lower than the modeling result, while the compressive stress results from the modeling was lower than the experimental results. At the measured positions, DANTE modeling predicted approximately 664 Mpa and − 183 Mpa maxima for draft tube immersion quench and intensively quenched conditions, respectively. This varied with the 181 Mpa and − 322 Mpa maxima measured experimentally from the draft tube immersion quenched and intensively quenched C-rings, respectively. The surface tensile residual stress was apparently overestimated, and the surface compressive residual stress was underestimated by DANTE simulations. Similar trends were observed by Juarez et al., in their study on the sensitivity of surface heat transfer coefficient on residual stress prediction accuracy in quenched 304L stainless steel from Jominy end quench experiment. Their modeling and experimental results varied. Maximum tensile residual stress was overestimated by about 20% by the FE model, and the maximum compressive residual stress was also underestimated by about the same percentage. However, their FE model predicted accurately the position of maxima. The FE model did not predict any significant change in residual stress distribution with any variance in HTC and temperature. (Ref 2, 28). In this present study, the discrepancy between the amount of the surface

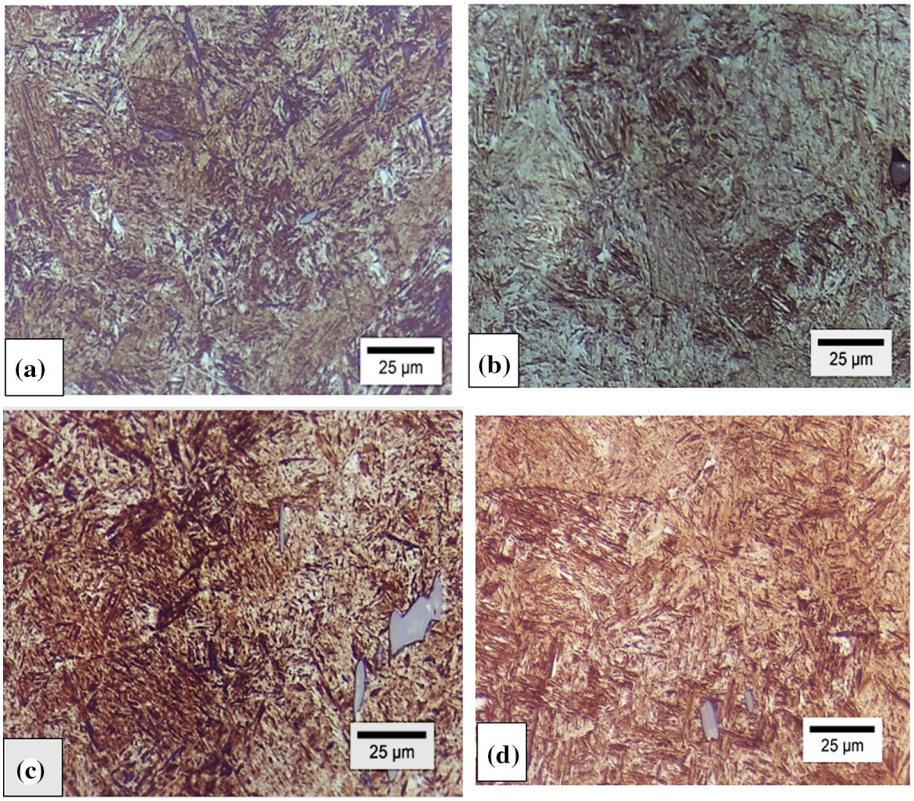

Fig. 11 Microstructure of the rings after quenching. Figures (a) and (b) are micrographs of the spray quenched sample taken from the thick and thin sections, respectively. While (c) and (d) are micrographs of the draft tube immersion quenched sample taken from the thick and thin sections, respectively. The gray features are MnS inclusions. Samples were etched with 2% Nital.

residual stresses predicted by the FE modeling and the experimentally measured values can be attributed to the fact that the FE modeling assumes elastic properties for the simulated material, while the experimental material exhibits elastoplastic behavior.

3.4 Distortion

Distortion and quality control are among the key issues in heat treatment industries (Ref 1). The presence of large thermal gradient during cooling results in contraction and difference in cooling rate across the sample. This leads to uneven thermal and transformation stress distribution in the sample. These quenching stresses could cause distortion, which is a dimensional variation such as bending, twisting, or warping, especially in the thin section of a material (Ref 1, 2, 29, 30). The distortion observed in the simulation was shape distortion in the x and z-directions; this could mean predominance of thermal stress in the quenched material. Thermal and transformation stress result in shape and size distortions, respectively (Ref 16, 30). Experimental measurement of distortion showed similar distortion trend to the simulation predictions for the percentage change in the fork gap opening along the x-direction. A percentage change of 1.5% and 1.4% was measured in the draft tube quenched and spray quenched C-rings, respectively (Fig. 14). However, DANTE simulation predicted twice the percent change in the fork gap opening along the x-direction in the spray quench modeling (0.9%) for the draft tube modeling result (1.7%). Hence, simulation and experimental results agree that there is less distortion in the intensively quenched C-rings than in the immersion quenched C-rings. Nonuniform cooling due to rewetting phenomena happening at the metal/quench medium interface is the chief cause of distortion and cracking during quenching. Samples parameter can significantly affect the heat transfer rate from sample surface during quenching and this affects temperature distribution, residual stress, and distortion in the sample. Such parameters include sample size, geometry, and material properties. Also, when high hardenability steel is quenched in a high quench severity medium, it increases the tendency of distortion and quench cracking because of high thermal stress (Ref 2).

3.5 Quench Cracks

Using the carbon equivalent, C_{eq}, equation developed by Kunitake and Susigawa (Ref 1), the steel composition gave C_{eq} of 0.63, confirming that the steel has medium sensitivity to cracking. Quench crack was observed in the samples quenched at 90° orientation from the spray nozzles. Samples quenched at 45° orientation from the nozzles did not crack. Hence, it can be deduced that 45° orientation of the rings allowed for uniform cooling of the part resulting in low thermal gradient and minimized pull stress on the surface of the ring. In the draft tube quench, two rings cracked from improper immersion. The cracks all developed along the same area of high tensile stress prediction and propagated along the thick section of the ring (Fig. 15). Sample properties such as geometry, composition, and surface conditions and heat-treating conditions such as nonuniform heating, wrong austenitization temperature, burning, overheating, and incorrect quenching contribute to quench cracks. Nonuniform cooling rate at the metal surface results in variation in contraction. There occurs a pull stress at the area of

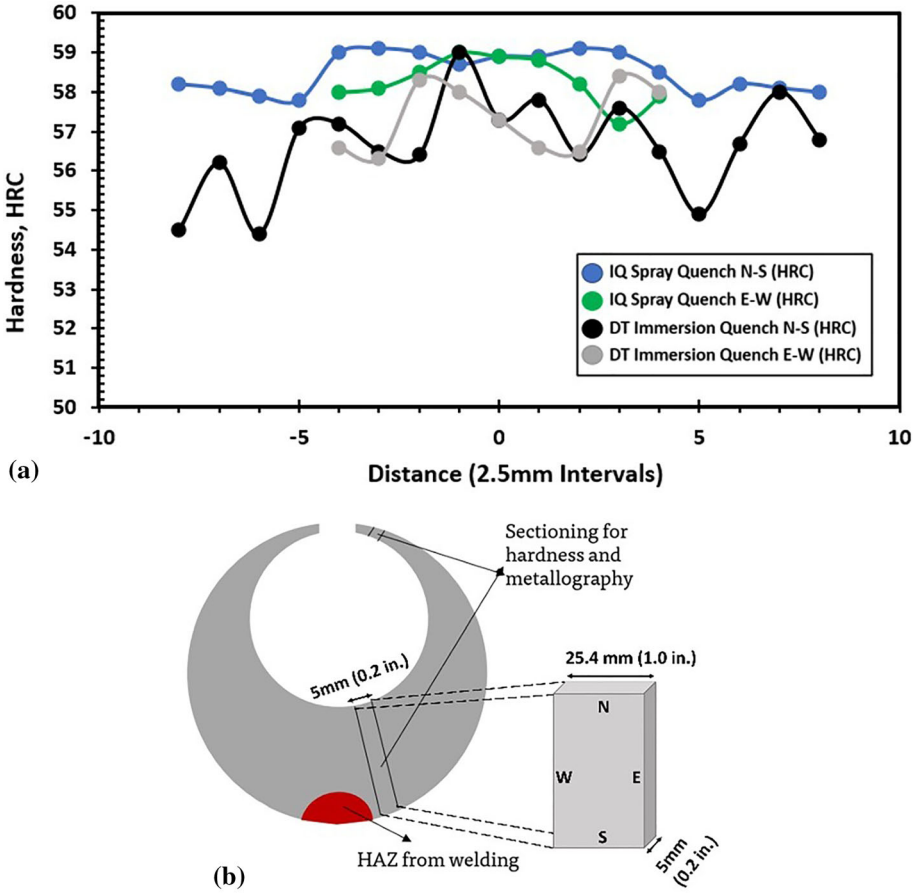

Fig. 12 (a) Shows the hardness profile of the thick section of DT (draft tube) immersion quench and IQ (intensively quenched) spray quenched C-rings. (b) A schematic of the C-ring showing hardness measurements directions: North-South (N-S) and East-West(E-W) directions, from a thick section

delay contraction with gradual cooling rate. This pull stress leads to pull cracking (Ref 1, 2).

Nonuniform cooling within the metal causes push or compressive stress in the region. While pull cracking is because of nonuniform cooling from austenitization temperature to martensite start temperature, push cracking is caused by nonuniform cooling within the martensitic transformation temperature range. Nevertheless, pull and push cracking occurs between M_s and M_f temperature range. Quench cracking in quenched materials is basically enabled by stress raisers such as sharp edges, rapid change in area, notches, holes, carbides, inclusions, and aggregates of impurities (Ref 1, 2). Volume increase during austenite–martensite phase transformation can create a stress system that when not constrained by the material, results in cracking in extreme conditions (Ref 1, 16).

4. Conclusion

This study has evaluated the key causes of quench defects and the effects of two different quench practices on quenched behaviors of materials including residual stress distribution, martensite transformation, distortion, and quench cracking. Hence, the following can be deduced:

a. The intensive quench system produced 30,000 W/m^{2}K HTC which was adequate to eliminate film boiling and nucleate boiling and promote uniform cooling of the surface of the ring, while the draft tube quench tank could only produce 14,000 W/m^{2}K.
b. The hardness and volume fraction of martensite transformation from the DANTE modeling, roughly correlated with the experimental data, with the intensive quench condition having a more uniform phase and hardness profile on the surface.
c. The draft tube immersion quench produced high tensile stress distribution on the surface of the ring compared to the intensive quench which yielded a large area coverage of compressive stress on the rings' surface. DANTE modeling overestimated the tensile stress and underestimated compressive stress measurements of the two quench conditions.
d. Quenched C-rings from the two quench practices distorted in different directions, with the immersion quench in the draft tube sample showing slightly higher distortion.
e. FE Simulation and experimental results suggest that rings quenched using immersion quench in the draft tube are more susceptible to cracking because of high surface ten-

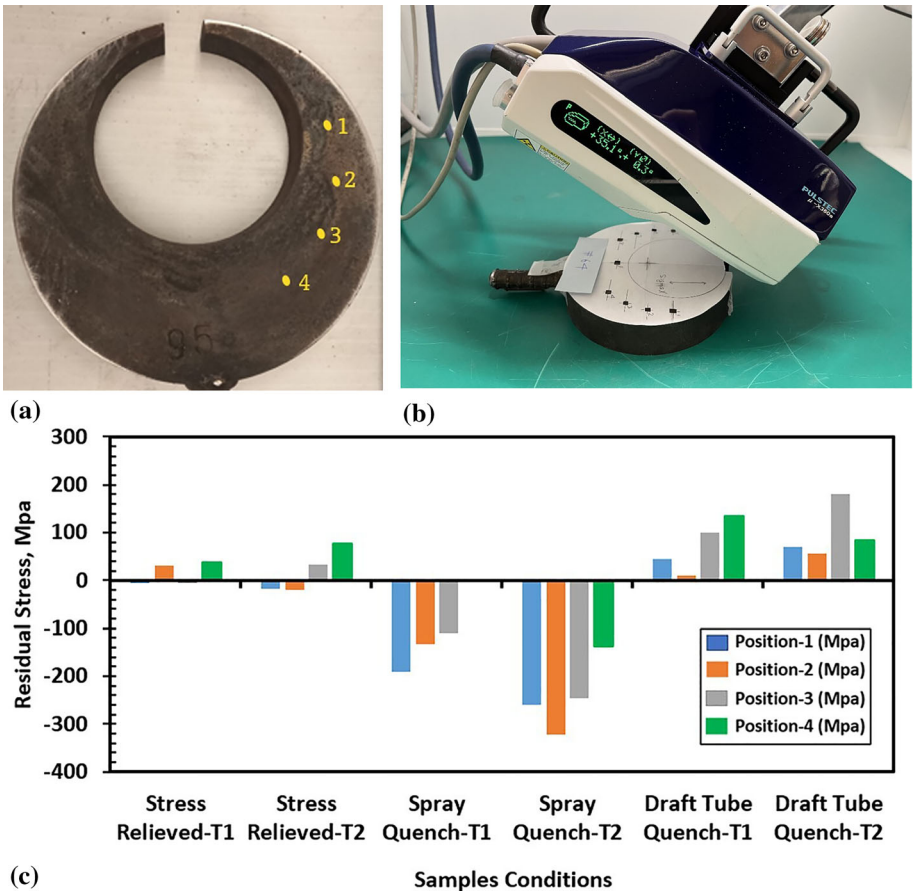

Fig 13 XRD results along the high stress distribution area on the C-rings for surface residual stress profile. (a) Measurement positions on the rings indicated on a quenched C-ring with no cracks. (b) Pulstec cos α technique residual stress measuring equipment. (c) surface residual stress plots of the stress relieved, IQ (spray quenched) and DT (draft tube immersion quenched) conditions. T1 and T2 represent trials 1 and 2, respectively. The two trials were done with similar conditions. The XRD result shows only a qualitative agreement with DANTE modeling prediction. Surface tensile residual stress appeared to be overestimated by DANTE modeling, while surface compressive residual stress was underestimated.

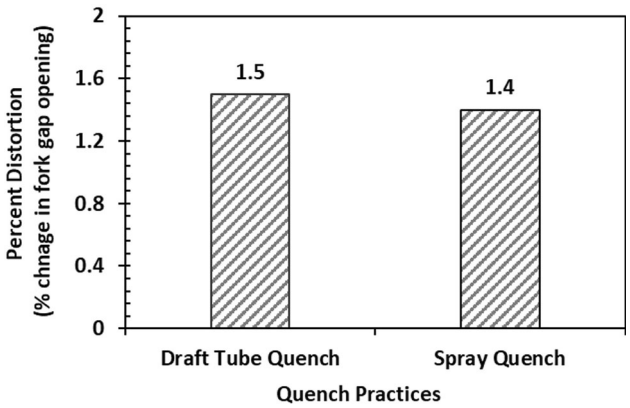

Fig. 14 Average distortion measured as the change in fork gap opening (ref. Fig. 3) of Navy C-ring water-quenched using forced convectional immersion quench in the draft tube (DT) and intensive quench (IQ) technique via spray quench system

sile stress concentration along the area of high bending moment. The high surface compressive stress distribution recorded on the ring quenched in the intensive quench spray tank would mean better dimensional stability.

Fig. 15 The cracked C-ring shows crack initiation corresponding with the area of high surface tensile residual stress distribution predicted in DANTE modeling

Acknowledgments

This AMC project was sponsored by the Defense Logistics Agency–Troop Support, Philadelphia, PA, and the Defense Logistics Agency Information Operations, J68, Research and Development, Ft. Belvoir, VA. The authors also wish to acknowledge the undergraduate students who participated in this work: Jackson Pointek, Joseph Boettcher, Jeremy Heisserer, and Nathan Davis.

Conflict of interest

The authors have no conflict of interest to declare.

References

1. L.C.F. Canale and G.E. Totten, Overview of Distortion and Residual Stress Due to Quench Processing Part I: Factors Affecting Quench Distortion, *Int. J. Materials and Product Technology*, 2005, **24**(1–4), p 4–52
2. A. Samuel and K.N. Prabhu, Residual Stress and Distortion during Quench Hardening of Steels: A Review, *J. of Materi Eng and Perform*, 2022, **31**, p 5161–5188
3. B. Hernandez-Morales, *Characterization of Heat Transfer During Quenching, Steel Heat Treating Fundamentals and Processes*, ASM Handbook, 2013
4. O. Anderoglu, Residual Stress Measurement using X-ray Diffraction, Doctoral Thesis, Texas A&M University, Brazos County, TX, USA, December 2004
5. D.E. Lozano, G.E. Totten, Y. Bedolla-Gil, M. Guerrero-Mata, M. Carpio, and G.M. Martinez-Cazares, X-ray Determination of Compressive Residual Stresses in Spring Steel Generated by High-Speed Water Quenching, *Materials*, 2019, **12**(7), p 1154. https://doi.org/10.3390/ma12071154
6. R.D. Lopez-Garcia, I. Medina-Juárez, and A. Maldonado Reyes, Effect of Quenching Parameters on Distortion Phenomena in AISI 4340 Steel, *Metals*, 2022, **12**, p 759
7. D. Easton, M. Perez, J. Huang, and S. Rahimi, Effects of Forming Route and Heat Treatment on the Distortion Behaviour of Case-Hardened Martensitic Steel type S156, 2017. https://strathprints.strath.ac.uk
8. B.E. Brooks and C. Beckermann, Prediction of Heat Treatment Distortion of Cast Steel C-Rings, Steel Founder's Society of America, paper No. 4.5, Chicago, IL, 2007
9. N. Kobasko, M. Aronov, J. Powell, and G. Totten, *Intensive Quenching Systems: Engineering and Design*, ASTM International, 2010. https://doi.org/10.1520/MNL64-EB
10. M.A. Aronov, *Intensive Quenching Technology for Heat Treating and Forging*, Final Technical Report. DOE Industrial Technologies Program, 2005
11. B. Liscis, *Intensive Quenching Technology*, Workshop on Quenching, Mangalore, 2008
12. M.A. Aronov, N.I. Kobasko, and J.A. Powell., Basic Principals, Properties and Metallurgy of Intensive Quenching, SAE International Journal of Materials and Manufacturing. March 2002
13. D.S. Mackenzie, *Advances in Quenching*, Gear Technology, 2005
14. M.A. Aronov, N.I. Kobasko, J.A. Powell, J.F. Wallace, and Y. Zhuo, Effect of Intensive Quenching on Mechanical Properties of Carbon and Alloy Steel, Proceedings of 23rd ASM Heat Treating Conference, Pittsburg, Pennsylvania, 2005
15. M. Aronov, N. Kobasko, J. Powell, W. Andreski, and J. Tirpak, Intensive Quenching for Lean Manufacturing of Steel Parts, *Adv. Mater. Processes*, 2017, **175**, p 56–60
16. M. Narazaki and G.E. Totten, Distortion of Heat-Treated Components, *Steel Heat Treatment: Metallurgy and Technology*. G.E. Totten Ed., Taylo & Francis Group, LLC, Boca Raton, 2006, p 608–650
17. Z. Li, B.L. Ferguson, X. Sun, P. Bauerle, Experiment and Simulation of Heat Treatment Results of C-Ring Test Specimen, Heat Treating: Proceedings of the 23rd Heat Treating Society Conference, September 25-28, 2005,
18. A. Duarte da Silva, T.A. Pedrosa, M.T. Aguilar, J. Schille, Z. Guo, and P.R. Cetlin, Distortion Prediction in Quenching AISI 4140 C-Rings with Different Quenchants, Technical contribution to 68th ABM International Congress, Belo Horizonte, MG, Brazil. July 30th to August 2nd, 2012
19. N. Cyril, B. Cyrille, L. Stéphane, T. Mihaela, and B. Régis, Comparison of Experimental and Simulation Distortions of Quenched C-Ring Test Parts, *Int. J. Mater. Form.*, 2009, **2**(S1), p 263–266. https://doi.org/10.1007/s12289-009-0484-y
20. Y. Haixuan, M. Yang, and R.D. Sisson, Application of C-Ring Specimen for Controlling the Distortion of Parts During quenching, *Metal Sci. Heat Treat.*, 2021, **63**(3–4), p 220–228. https://doi.org/10.1007/s11041-021-00674-w
21. M.M. Nunes, E. Miguel, R. da Silva, A. Renzetti, and T.G. Brito, Analysis of Quenching Parameters in AISI 4340 Steel by Using Design of Experiments, *Mater. Res.*, 2018 https://doi.org/10.1590/1980-5373-mr-2018-0315
22. H. Farivar, U. Prahl, M. Hans, and W. Bleck, Microstructural Adjustment of Carburized Steel Components Towards Reducing the Quenching-induced Distortion, *J. Mater. Process. Technol.*, 2019, **264**, p 313–327
23. K. Tanaka and Y. Akiniwa, Diffraction Measurements of Residual Macrostress and Microstress Using X-Rays, Synchrotron and Neutrons, *JSME Int. J. Ser. A*, 2004, **47**, p 252
24. D. Delbergue, D. Texier, M. Levesque, and P. Bocher, Comparison of Two X-Ray Residual Stress Measurement Methods: $Sin^2\ \psi$ and Cos α, Through the Determination of a Martensitic Steel X-Ray Elastic Constant, Residual Stresses 2016: ICRS-10 , Jul 2016, Sydney, Australia
25. D. Delbergue, X-Ray Diffraction for Residual Stress and Cold Work measurements of Short Peened Materials, Doctoral Thesis. École De Technologie Supérieure Université du Québec, 2020
26. ASM handbook "Heat Treating" Vol.4, 10th edition. 1991
27. M. Sedighi and M.M. Salek, Modeling and Experimental Study of Quenching Process for Aisi 4340 Aeronautical Steel Under Different Cooling Conditions, *Trans. Can. Soc. Mech. Eng.*, 2008, **32**(1), p 1–8
28. I. Medina-Juárez, J. Araujo De Oliveira, R.J. Moat, and F.A. García Pastor, On the Accuracy of Finite Element Models Predicting Residual Stresses in Quenched Stainless Steel, *Metals*, 2019, **9**(12), p 1–16
29. T.M. Sonar and S.V. Lomte, Effect of Deep Cryogenic Treatment on Surface Integrity and Dimensional Stability of D2 Tool Steel, *IJRET.*, 2015, **4**(8), p 67–71
30. S. Kamamoto, T. Nishimori, and S. Kinoshita, Analysis of Residual Stress and Distortion Resulting from Quenching in Large Low-alloy Steel Shafts, *Mater. Sci. Technol. (United Kingdom)*, 1985, **1**(10), p 798–804